VIETNAM NATIONAL UNIVERSITY, HANOI

UNIVERSITY OF SCIENCE

.

Pham The An

IMPROVEMENTS OF CRITICAL CURRENT DENSITY OF Bi-Pb-Sr-Ca-Cu-O HIGH-T_c SUPERCONDUCTOR BY ADDITIONS OF NANO-STRUCTURED PINNING CENTERS

Major: Thermophysics

Code: 9440130.07

DISSERTATION SUMMARY FOR DOCTOR OF PHILOSOPHY IN PHYSICS

Ha Noi – 2023

ABSTRACT

The objective of this dissertation is to systematically investigate the impact of pinning center additions on the enhancement of the critical current density (J_c) and the flux pinning mechanism improvements in $Bi_{1.6}Pb_{0.4}Sr_2Ca_2Cu_3O_{10+\delta}$ polycrystalline superconductors. Specifically, $Bi_{1.6}Pb_{0.4}Sr_2Ca_2Cu_3O_{10+\delta}$ polycrystalline superconductors were synthesized using conventional solid state reaction methods, and the collective pinning theory was applied to gain insight into intrinsic pinning properties and improvements to J_c in the Bi-Pb-Sr-Ca-Cu-O (BPSCCO) system. This dissertation presents an investigation into the J_c and pinning mechanism in BPSCCO superconductors. Additionally, various types of nano-sized pinning centers, including point-like defects, non-magnetic, and magnetic nanoparticles, were added to BPSCCO samples to further investigate their effects.

CHAPTER 1: OVERVIEW

Given the research context as presented, along with the limitations of the BPSCCO system, the dissertation aims to enhance J_c and flux pinning of BPSCCO superconductors through the manipulation of pinning addition effects. The dissertation studies and addresses about the issues:

- Fabricate $Bi_{1.6}Pb_{0.4}Sr_2Ca_2Cu_3O_{10+\delta}$ samples with alkali metal substitutions to investigate the effect of point-like pinning on J_c of the samples. The theoretical models of collective pinning and flux pinning mechanism will be applied to investigate the additional pinning in the substituted samples.
- Fabricate $Bi_{1.6}Pb_{0.4}Sr_2Ca_2Cu_3O_{10+\delta}$ samples with semiconducting nanoparticles to enhance J_c and flux pinning proper-

ties of the samples. The influence of non-magnetic nanoparticles on crystal structure, local structure and critical properties will be investigated systematically. The significant decrease of T_c could relate to the variation in local structure and was investigated by L-D model and XAS analysis. The behaviors of nanoparticle as the dopant on flux pinning mechanism will be examined. Especially, the geometry of additional pinning centers will be identified by the Dew-Hughes model.

- Fabricate $Bi_{1.6}Pb_{0.4}Sr_2Ca_2Cu_3O_{10+\delta}$ samples with magnetic nanoparticles to enhance J_c and flux pinning properties of the samples. The influence of ferromagnetic nanoparticles on crystal structure and critical properties of the superconductor system will be investigated. The geometry of additional pinning centers will be identified by the Dew-Hughes model. The pinning potential will be presented as more confident evidence for magnetic dopant on the J_c and flux pinning enhancement.

CHAPTER 2: EXPERIMENTS

2.1. SAMPLE FABRICATIONS

2.1.1 Fabrication of Bi-Pb-Sr-Ca-Cu-O polycrystalline samples

The sample of stoichiometry of $Bi_{1.6}Pb_{0.4}Sr_2Ca_2Cu_3O_{10+\delta}$ were prepared by the conventional solid-state reaction technique.

2.1.2. Fabrication of nanoparticles

2.1.2.1. The Titanium dioxide nanoparticle

Semiconducting TiO_2 nanoparticles were prepared by the hydrothermal route.

2.1.2.2. The Iron(II,III) oxide nanoparticle

Fe_3O_4 nanoparticles were synthesized by the chemical co-precipitation route.

2.1.3. Introductions of pinning centers into Bi-Pb-Sr-Ca-Cu-O polycrystalline samples

The completed fabrication process was illustrated in Figure. 2.1.

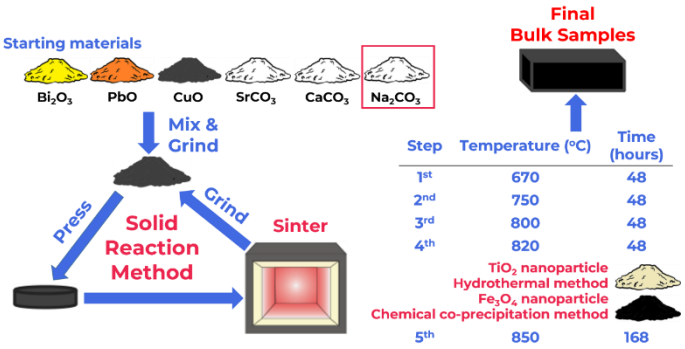

Figure 2.1. Fabrication process of sample series illustration

2.2. SAMPLE CHARACTERIZATIONS

CHAPTER 3: IMPROVEMENTS OF CRITICAL CURRENT DENSITY IN HIGH-T_c $Bi_{1.6}Pb_{0.4}Sr_2Ca_2Cu_3O_{10+\delta}$ OF SUPERCONDUCTOR BY USING SUBSTITUTION EFFECT

3.1. FORMATION OF THE SUPERCONDUCTING PHASES

3.2. IMPROVEMENTS OF J_c

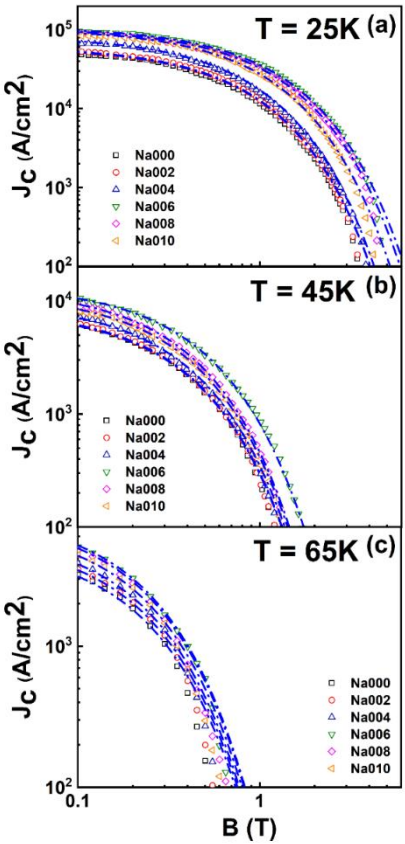

Figure 3.1. Descriptions of the field dependence of J_c of all samples by using the collective pinning theory at (a) 65 K, (b) 45K and (c) 25 K. The solid lines are the fitting curves using Eq. (1.2)

It would be clearly seen that the enhancements of J_c are obtained in all Na-substituted samples. In particular, the J_c was enhanced from Na002, reached a maximum at Na006, and then decreased for Na008 and Na010 samples.

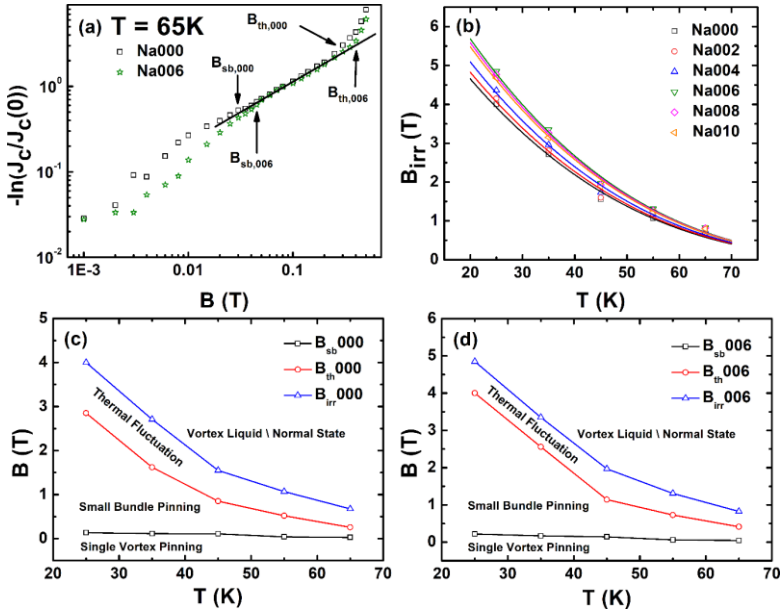

Figure 3.2. (a) Field dependence of -ln($J_c(B)/J_c(0)$) of Na000 and Na006 samples at 65K. (b) The temperature dependence of B_{irr} of all samples at different temperatures. The solid lines are the fitting curves using Eq. (3.1). (c) The B-T phase diagram of Na000 sample. (d) The B-T phase diagram of Na006 sample

The enlargements of single vortex pinning, and small bundle pinning regions would attribute to the enhancements of the flux pinning properties in the Na006 sample, which were provided by Na substitution.

3.3. FLUX PINNING PROPERTIES

3.3.1. Improvements of pinning force density

3.3.2. Identification of flux pinning type

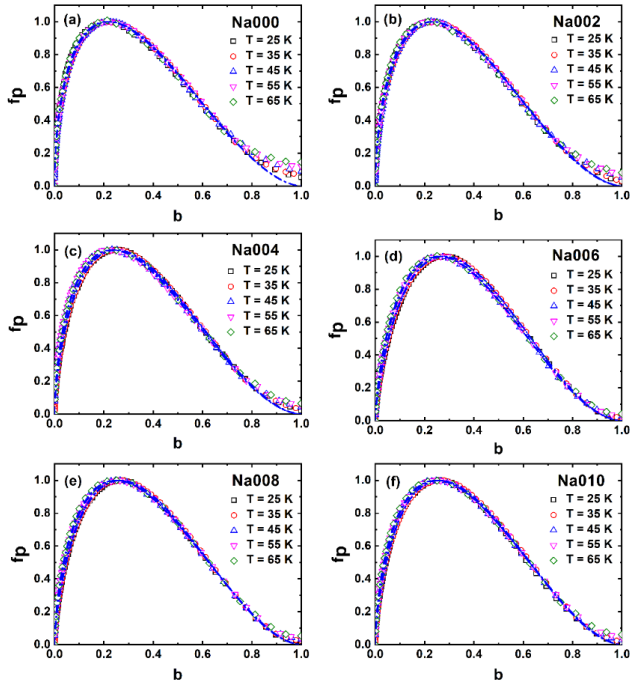

Figure 3.3. Scaling behaviors of the normalized pinning force density (f_p) versus (b) at all measured temperatures of (a) Na000, (b) Na002, (c) Na004, (d) Na006, (e) Na008 and (f) Na010 samples. The solid lines are the fitting curves using Eq. (1.7).

The maximum p and q were achieved on Na006 sample, which are 0.70 and 1.92, respectively. Moreover, these results also pointed out that the core interaction was the predominant pinning mechanism in all samples as predicted by Dew-Hughes. A possible explanation for

these phenomena might be related to the fact that Na^+ was successfully partially substituted into Ca sites.

3.3.3. Flux pinning mechanism

To generalize, the homogeneity of the collective pinning model and Dew-Hughes model indicated that the 0D punctual defects created by the partial Na substitution provided J_c enhancement with the δl core interaction in a wide range of temperature and field via flux pinning mechanism.

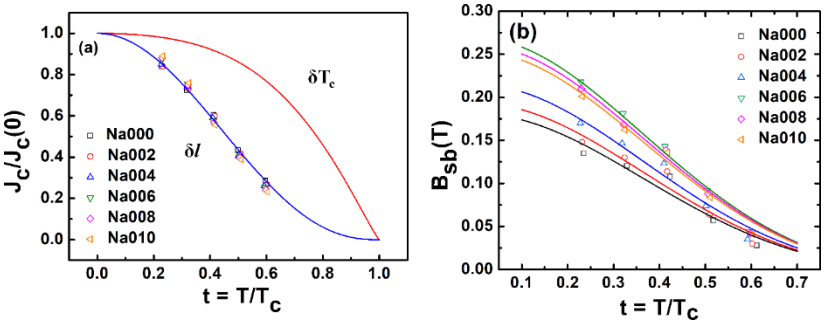

Figure 3.4. (a) Normalized critical current density $J_c(t)/J_c(0)$ versus normalized temperature t of all the samples; (b) Crossover field (B_{sb}) versus normalized temperature of all the samples. The solid lines are the fitting curves using Eq. 1.5.

3.4. CONCLUSION OF CHAPTER 3

In this chapter, the scaling behaviour of flux pinning forces in $Bi_{1.6}Pb_{0.4}Sr_2Ca_{2-x}Na_xCu_3O_{10+\delta}$ superconductors was systematically investigated. It was found that the magnetic field dependence of J_c at different temperatures ranged between 65 K and 25 K was significantly enhanced by the Na substitution via point-like defect creations. This field dependence of J_c was well described using the collective

pinning theory. The *B*-*T* phase diagrams were constructed. The improved flux pinning properties in the Na-substituted samples were evident from comparing the fitting values of p, q and b_{peak} following the Dew-Hughes model.

CHAPTER 4: IMPROVEMENTS OF CRITICAL CURRENT DENSITY IN HIGH-T_c $Bi_{1.6}Pb_{0.4}Sr_2Ca_2Cu_3O_{10+\delta}$ SUPERCONDUCTOR BY ADDITION OF NON-MAGNETIC NANOPARTICLES

4.1. NANOPARTICLE CHARACTERISTICS

The particles were nearly spherical nanomaterials with crystallite sizes in the range of 4-22 nm. The average size of the TiO_2 nanoparticles was around 12 nm.

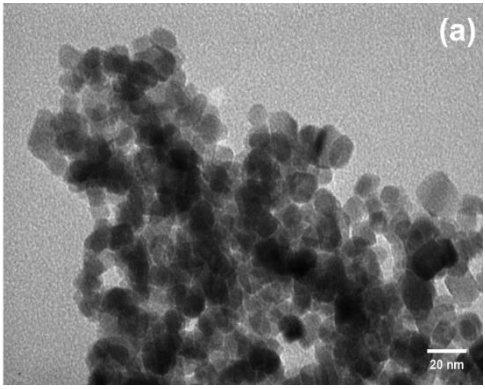

Figure 4.1. (a) TEM images and (b) histogram of TiO_2 nanoparticles

4.2. FORMATION OF THE SUPERCONDUCTING PHASES

4.2.1. Phase analysis

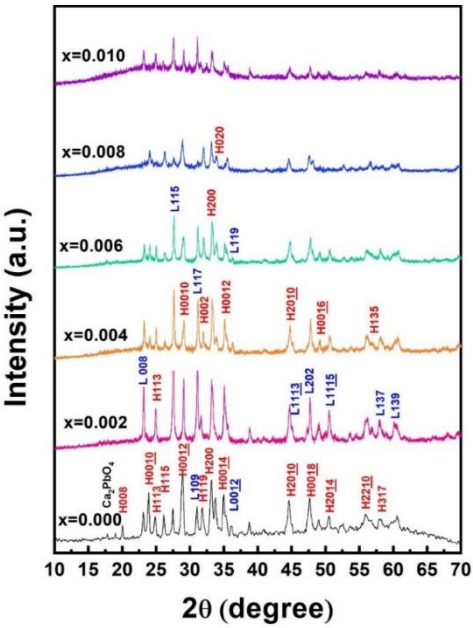

Figure 4.2. XRD patterns of $(Bi_{1.6}Pb_{0.4}Sr_2Ca_2Cu_3O_{10+\delta})_{1-x}(TiO_2)_x$ samples, with x = 0, 0.002, 0.004, 0.006, 0.008, and 0.0104.

The volume fraction values showed that *%Bi-2223* was decreased, whereas *%Bi-2212* was increased monotonously by increasing the TiO_2 content. The volume fraction and crystallite size investigation results revealed that TiO_2 nanoparticle decelerated Bi-2223 phase formation. The lattice parameters were around $a = b = 5.395 \pm 0.007$ Å and $c = 37.07 \pm 0.01$ Å relating to the tetragonal structure.

4.3. THE CORRELATION BETWEEN LOCAL STRUCTURE VARIATIONS AND CRITICAL TEMPERATURE

4.3.1. Critical temperature

The T_c of the samples was decreased by the addition of TiO_2. The value of ρ_0 is extrapolated and presented in Table 4.1. The ρ_0 is increased gradually with x = 0.002, 0.004. From x = 0.006, the value of ρ_0 increases more strongly; when x = 0.010, the ρ_0 is about thrice higher than that in the pure sample.

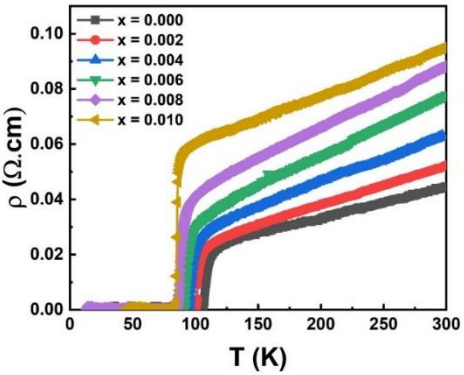

Figure 4.3. The temperature dependence of resistivity of $(Bi_{1.6}Pb_{0.4}Sr_2Ca_2Cu_3O_{10+\delta})_{1-x}(TiO_2)_x$ samples, with x = 0, 0.002, 0.004, 0.006, 0.008, and 0.010

4.3.2. Fluctuation of mean field region

The coherence length and effective inter-layering spacing increased with increasing doping content. This result explains the reduction in the superconducting properties of the material in the CuO_2 interlayer. Nevertheless, the remarkable decrease in T_c with increasing TiO_2

content may be ascribed to other factors.

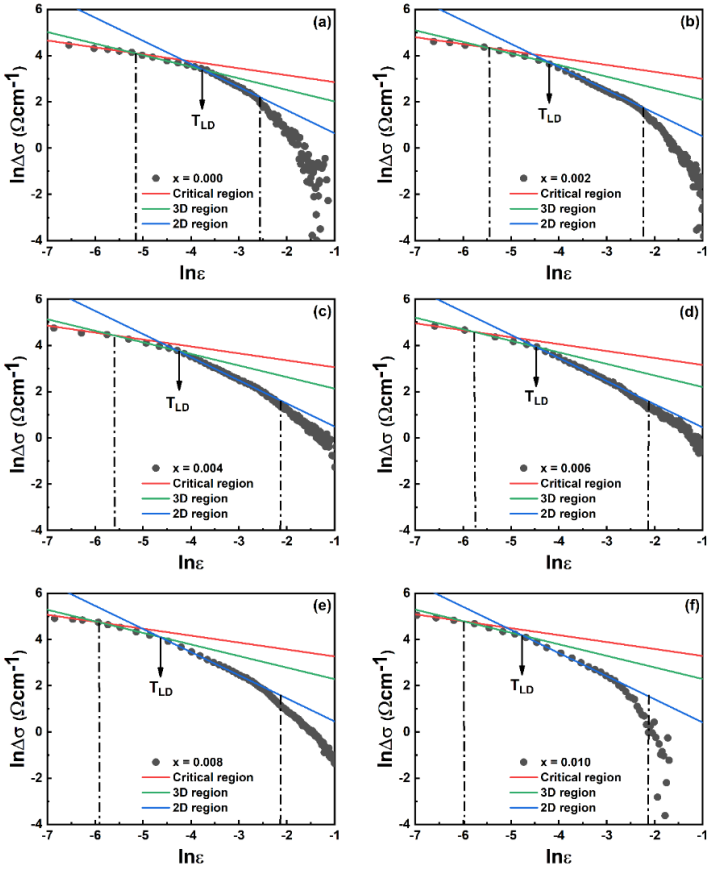

Figure 4.4. Double logarithmic plot of excess conductivity as a function of reduced temperature of $(Bi_{1.6}Pb_{0.4}Sr_2Ca_2Cu_3O_{10+\delta})_{1-x}(TiO_2)_x$ samples (a) $x = 0$, (b) $x = 0.002$, (c) $x = 0.004$, (d) $x = 0.006$, (e) $x = 0.008$, and (f) $x = 0.010$. The red, green, and blue solid lines correspond to the critical region, 3D and 2D region, respectively

4.3.3. Local structure variations

The Cu $L_{2,3}$-edge spectra for all samples are plotted in Figure 4.8(a). The carrier concentration in the conducting planes was calculated from the XANES spectra of Cu $L_{2,3}$-edge. The measurement was conducted at room temperature, and the energy was set from 920 eV to 980 eV. Two main peaks appeared at approximately 933 and 955 eV

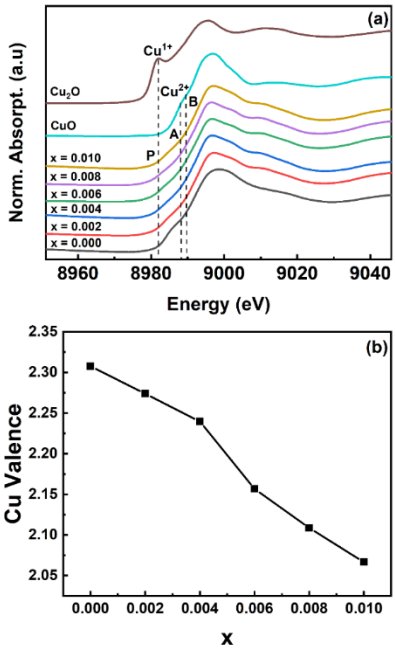

for all samples. I determined the intensities of the main and shoulder peaks from the fitting of L_3 spectra and applied them to the following equation: $p = I(Cu^{3+})/(I(Cu^{2+}) + I(Cu^{3+}))$, where $I(Cu^{2+})$ and $I(Cu^{3+})$ are the integrated intensities of the main and shoulder peaks, respectively.

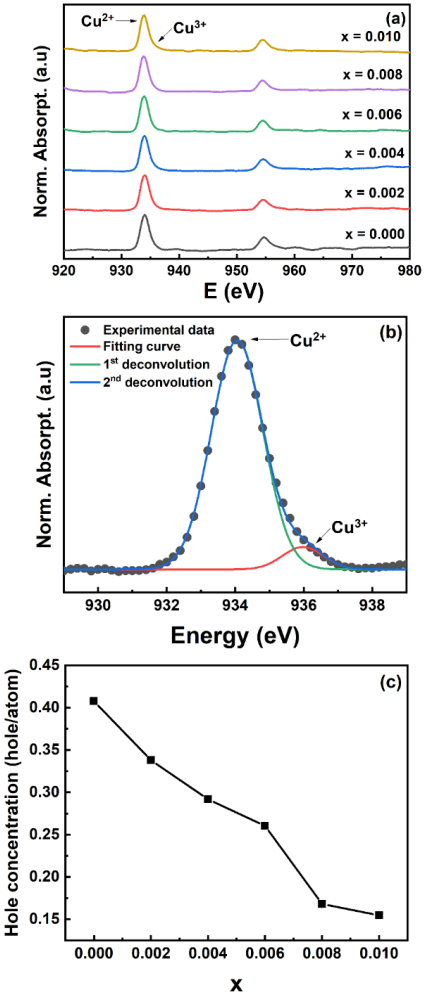

Figure 4.5. (a) Cu K-edge XANES spectra of $(Bi_{1.6}Pb_{0.4}Sr_2Ca_2Cu_3O_{10+\delta})_{1-x}(TiO_2)_x$ samples, with x = 0, 0.002, 0.004, 0.006, 0.008, and 0.010. (b) Copper valence of all samples

4.4. IMPROVEMENTS OF J_c

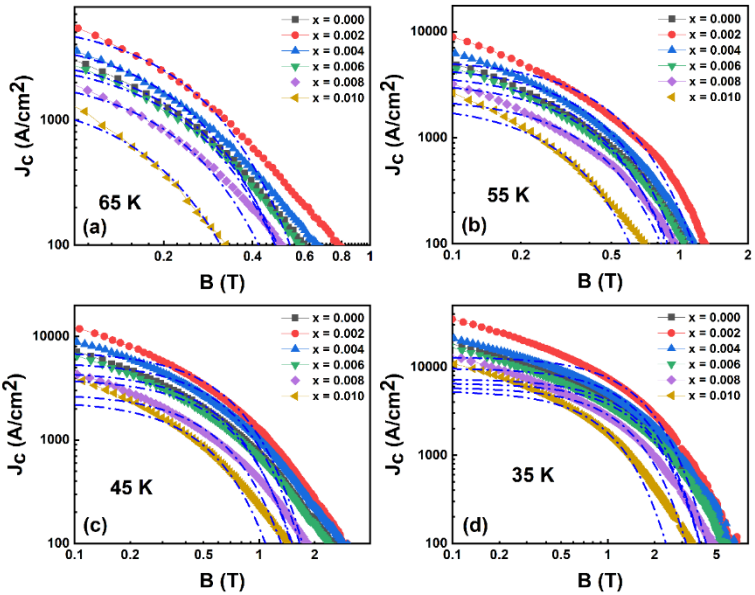

Figure 4.6. The field dependence of J_c of $(Bi_{1.6}Pb_{0.4}Sr_2Ca_2Cu_3O_{10+\delta})_{1-x}(TiO_2)_x$ samples, with x = 0, 0.002, 0.004, 0.006, 0.008, and 0.010 with small bundle regimes description using collective pinning theory at (a) 65 K, (b) 55 K, (c) 45 K, and (d) 35 K. Dash-dot lines are fitting curves using Equation (1.2)

Specifically, optimal J_c enhancement was obtained at a dopant amount of x = 0.002 and slightly decreased in the x = 0.004 sample. Furthermore, when all samples were compared, J_c descended much slower under the applied field on these samples. conditions with the proper amount of doping content [14,49,58,96].

First, in the single vortex regime, where the vortices are individually pinned, the J_c in field is nearly plateau. On x = 0.002 and x = 0.004, the plateau J_c was wider, which could prove the increment in pinning

center quantity. With increasing magnetic field, the vortex density became greater than the pinning center density; then, the vortices started to be collectively pinned [7,9,23,84]. Therefore, the extension of the single vortex regime was probably indicated by the appearance of additional nano-defects as additional pinning centers [23,43,84]. These artificial pinning centers also revealed a good collective pinning ability via the extension of the small bundle regime.

4.5. FLUX PINNING PROPERTIES

4.5.1. Flux pinning mechanism

The natural pinning center is defined as grain boundaries on the pure sample, and δl pinning is reasonable for this type of center. The additional pinning centers were also predicted to provide fluctuation in the mean free path of the charge carrier, which is related to the defects, distortions, and dislocations.

Figure 4.7. (a) The normalized temperature dependence of normalized J_c and (b) normalized B_{sb} of $(Bi_{1.6}Pb_{0.4}Sr_2Ca_2Cu_3O_{10+\delta})_{1-x}(TiO_2)_x$ samples, with x = 0, 0.002, 0.004, 0.006, 0.008, and 0.010. Solid lines are fitting curves in terms of the δl pinning and δT_c pinning mechanisms using Eqs. 1.5 and 1.6

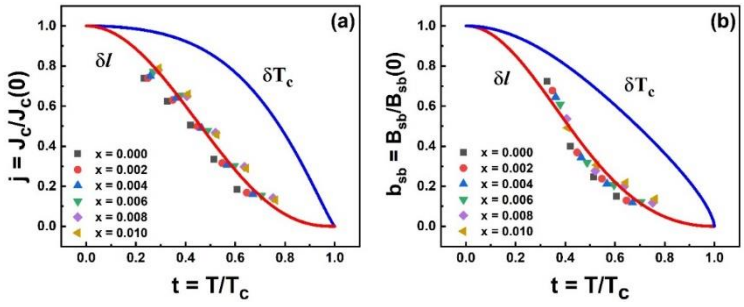

4.5.2. Improvements of pinning force density

4.5.3. Identification of flux pinning center

Compared with the inter-flux-line spacing $d = 1.07(\Phi_0/B)^{1/2}$, the average size of TiO_2 nanoparticles was smaller than that in all investigated range of magnetic field [11,80]. Therefore, the geometry of center was satisfied as point-like pinning center. Hence, the doped TiO2 nanoparticles operated as the normal core point pinning centers on doped samples, corresponding to $p = 1$ and $q = 2$ in Dew-Hughes's model [11,30].

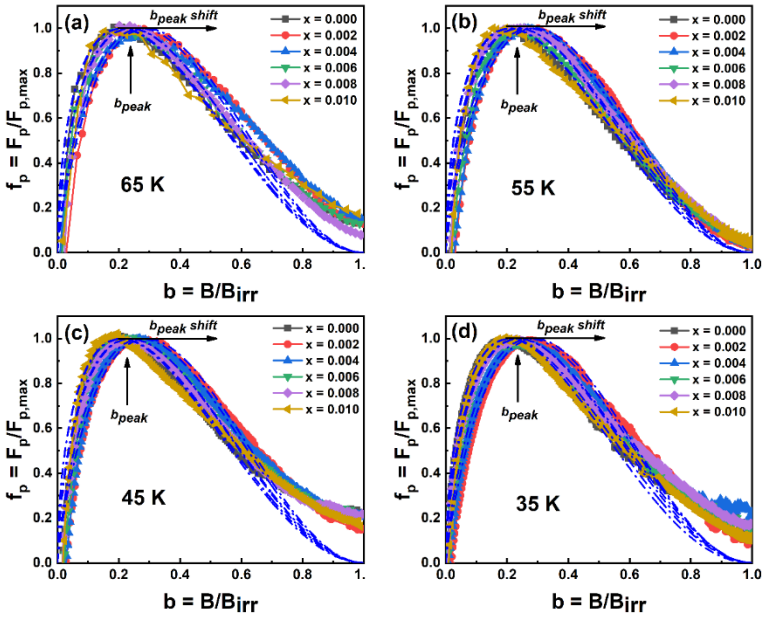

Figure 4.8. The normalized field dependence of $(Bi_{1.6}Pb_{0.4}Sr_2Ca_2Cu_3O_{10+\delta})_{1-x}(TiO_2)_x$ samples, with $x = 0$, 0.002, 0.004, 0.006, 0.008, and 0.010 with modified Dew-Hughes model scaling at (a) 65 K, (b) 55 K, (c) 45 K ,and (d) 35 K. Solid lines are

fitting curves using Eq. 1.7.

4.6. CONCLUSION OF CHAPTER 4

The effects of TiO_2 nanoparticles on the structure, morphology, critical and flux pinning properties of $Bi_{1.6}Pb_{0.4}Sr_2Ca_2Cu_3O_{10+\delta}$ superconductor were systematically investigated. The excess conductivity in the framework of the A–L and L–D theory analyses displayed that the mean field region was fluctuated by TiO_2 with increasing c-axis coherence length and effective CuO_2 interlayer spacing. The reduction in both Cu valence state and hole concentration on the doped sample was probed by using Cu K-edge and Cu $L_{2,3}$-edge XANES spectra. The $J_c(B)$ of the samples were enhanced by adequate doping contents of x = 0.002, 0.004. The values of B_{sb} and B_{lb} were estimated for all samples at 65, 55, 45, and 35 K. The results revealed the extension of the small and large bundle regimes with adequate amounts of TiO_2 nanoparticles. The $j(t)$ analyses exhibited that the δl pinning was the dominant pinning mechanism in all samples. The increasing p fitting parameter increase on x = 0.002 and 0.004 samples exhibited that the additional centers were normal core point pinning centers.

CHAPTER 5: IMPROVEMENTS OF CRITICAL CURRENT DENSITY IN HIGH-T_c $Bi_{1.6}Pb_{0.4}Sr_2Ca_2Cu_3O_{10+\delta}$ SUPERCONDUCTOR BY ADDITION OF MAGNETIC NANOPARTICLES

5.1. NANOPARTICLE CHARACTERISTICS

The nanoparticles were found to be mostly in spherical form and its average size was about 19 nm.

5.2. FORMATION OF THE SUPERCONDUCTING PHASES

5.2.1. Phase analysis

The %Bi-2223 phase monotonously decreased, whereas the %Bi-2212 phase increased with the increase in doping content. The average crystallite size continuously decreased as the doping content was increased. Therefore, Fe_3O_4 nanoparticles possibly decelerated the Bi-2223 phase formation.

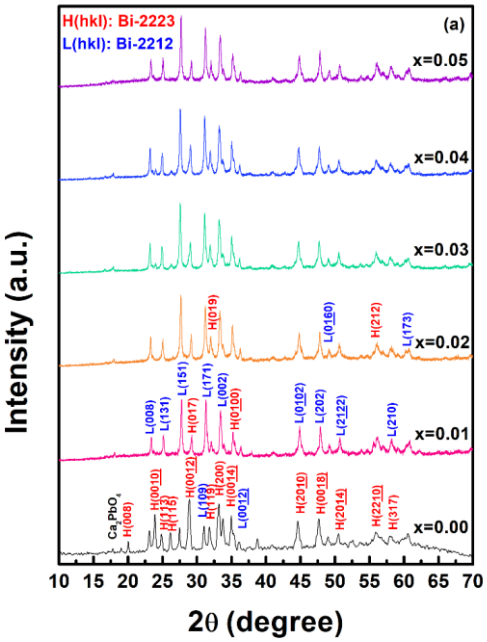

Figure 5.1. (a) XRD patterns and (b) Volume fractions and average crystalline size of $(Bi_{1.6}Pb_{0.4}Sr_2Ca_2Cu_3O_{10+\delta})_{1-x}(Fe_3O_4)_x$ samples, with x = 0, 0.01, 0.02, 0.03, 0.04, and 0.05

5.2.2. Surface morphology

5.3. IMPROVEMENTS OF J_c

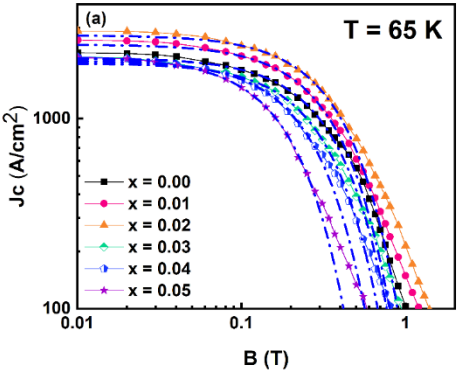

Figure 5.2. (a) Field dependence of J_c at 65 K with small-bundle regime fitting in double-logarithmic scale, (b) field dependence of $-\ln[J_c(B)/J_c(0)]$ of the x = 0 and 0.02 samples

The results revealed that the J_c values of the doped samples increased for x = 0.01 and 0.02 and gradually decreased for $x \geq 0.03$. The strongest J_c enhancement was obtained on the x = 0.02 sample.

5.4. FLUX PINNING PROPERTIES

5.4.1. Identification of pinning center

For the x = 0.01 and 0.02 samples, the value of p increased from 0.5537 to 0.6523 and 0.6695, and the value of b_{peak} increased from 0.2168 to 0.2459 and 0.2508, respectively, with both exhibiting the point-like pinning mechanism (b_{peak} = 1/3) [11].

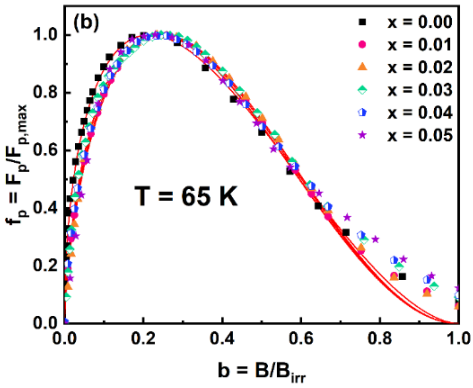

Figure 5.3. (a) Normalized field dependence of F_p at 65 K, (b) normalized field dependence of f_p with Dew–Hughes model fitting of $(Bi_{1.6}Pb_{0.4}Sr_2Ca_2Cu_3O_{10+\delta})_{1-x}(Fe_3O_4)_x$ samples, with x = 0, 0.01, 0.02, 0.03, 0.04, and 0.05

5.4.2. Improvements of pinning potential

The precipitates at grain boundaries improve U_0 of Bi-2212 bulks. Possible reasons for the enhancements were attributed to: (i) the improved pinning force F_p and (ii) and strengthened activation energy U_0.

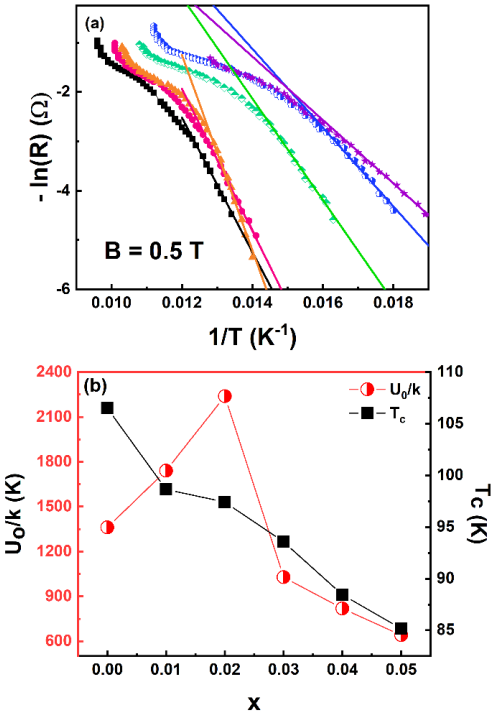

Figure 5.4. (a) Arrhenius plot at 0.5T using Equation (5.1), and (b) Pinning potential and T_c of $(Bi_{1.6}Pb_{0.4}Sr_2Ca_2Cu_3O_{10+\delta})_{1-x}(Fe_3O_4)_x$ samples, with x = 0, 0.01, 0.02, 0.03, 0.04, and 0.05

5.5. COMPARISON OF SUBSTITUTION EFFECT, NONMAGNETIC AND MAGNETIC NANOPARTICLES DOPING ON THE CRITICAL CURRENT DENSITY OF Bi1.6Pb0.4Sr2Ca2Cu3O10+δ CERAMIC SUPERCONDUCTOR

The results illustrate that the highest enhancement of J_c was achieved by the addition of Fe_3O_4 magnetic nanoparticles with $x = 0.02$.

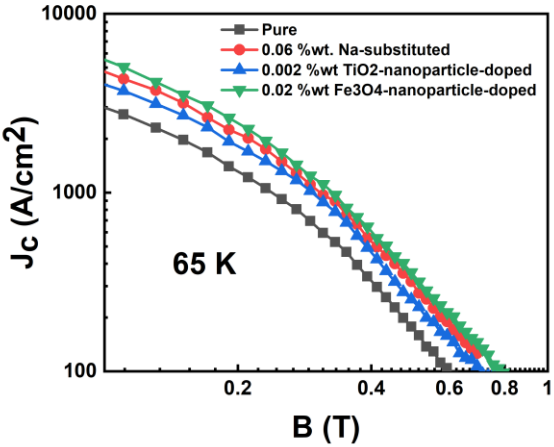

Figure 5.5. The field dependence of J_c at the optimal content of Na-substituted, TiO_2-nanoparticle-doped, and Fe_3O_4-nanoparticle-doped $Bi_{1.6}Pb_{0.4}Sr_2Ca_2Cu_3O_{10+\delta}$ superconductor

CONCLUSIONS

In this dissertation, the explorations of issue of critical current density and pinning mechanism in Bi-Pb-Sr-Ca-Cu-O superconductors were carried out. Main results of this dissertation, improvements of J_c in BPSCCO superconductors, might be summarized as the followings:

The improved flux pinning properties in the Na-substituted samples were evident from comparing the fitting values of p, q and b_{peak} following the Dew-Hughes model. The obtained data also demonstrated the growth of point-like pinning and the decline of grain boundary pinning resulting from the Na substitution. Especially, the δl pinning was found to be the predominant pinning mechanism responsible for the samples, which was related to spatial variations in the mean free

path of charge carriers.

For the BPSCCO superconductors with the addition of non-magnetic TiO_2 nanoparticles, the $J_c(B)$ of the samples were enhanced by adequate doping contents of x = 0.002, 0.004. The results revealed the extension of the small and large bundle regimes with adequate amounts of TiO_2 nanoparticles. The $j(t)$ analyses exhibited that the δl pinning was the dominant pinning mechanism in all samples. The increasing p fitting parameter increase on x = 0.002 and 0.004 samples exhibited that the additional centers were normal core point pinning centers. Additionally, a close correlation between local structural variations and change in T_c of the BPSCCO was investigated. The reduction in both Cu valence state and hole concentration on the doped sample probed by using Cu K-edge and Cu $L_{2,3}$-edge XANES spectra was probably attributed to the observed decrease in T_c of the nanoparticle added BPSCCO superconductors.

For the BPSCCO samples with the additions of magnetic Fe_3O_4 nanoparticles, the enhancements of J_c were obtained for x = 0.01 and 0.02. Possible reasons for the enhancements were attributed to: (i) the improved pinning force and (ii) and strengthened activation energy. The appearance of additional normal core point pinning centers in the doped samples was confirmed by using the Dew–Hughes model. Interestingly, the additions of magnetic nanoparticles were concluded to provide the strongest enhancements of J_c among the methods used in the research.

DISSERTATION PUBLICATIONS

[1] **An T. Pham**, Dzung T. Tran, Duong B. Tran, Luu T. Tai, Nguyen K. Man, Nguyen T. M. Hong, Tien M. Le, Duong Pham, Won-Nam Kang, Duc H. Tran (2021), "Unravelling the scaling characteristics of flux pinning forces in $Bi_{1.6}Pb_{0.4}Sr_2Ca_{2-x}Na_xCu_3O_{10+\delta}$ superconductors", Journal of Electronics Materials 50, pp. 1444-1451.

[2] **An T. Pham**, Dzung T. Tran, Ha H. Pham, Nguyen H. Nam, Luu T. Tai, Duc H. Tran (2021), "Improvement of flux pinning properties in Fe_3O_4 nanoparticle-doped $Bi_{1.6}Pb_{0.4}Sr_2Ca_2Cu_3O_{10+\delta}$ superconductors", Materials Letters 298, pp. 130015(1-5).

[3] **An T. Pham**, Dzung T. Tran, Linh H. Vu, Nang T.T. Chu, Nguyen Duy Thien, Nguyen H. Nam, Nguyen Thanh Binh, Luu T. Tai, Nguyen T.M. Hong, Nguyen Thanh Long, Duc H. Tran (2022), "Effects of TiO_2 nanoparticle addition on the flux pinning properties of the $Bi_{1.6}Pb_{0.4}Sr_2Ca_2Cu_3O_{10+\delta}$ ceramics", Ceramics International 48(14), pp. 20996–21004.

[4] **An T. Pham**, Linh H. Vu, Dzung T. Tran, Nguyen Duy Thien, Wantana Klysubun, T. Miyanaga, Nguyen K. Man, Nhan T.T. Duong, Nguyen Thanh Long, Phong V. Pham, Nguyen Thanh Binh, Duc H. Tran (2023), "Correlation between local structure variations and critical temperature of $(Bi_{1.6}Pb_{0.4}Sr_2Ca_2Cu_3O_{10+\delta})_{1-x}(TiO_2)_x$ superconductor", Ceramics International 49(7), pp. 10506-10512.